haclacHAC-LACHigh Authority Control - Low Authority Control hacHACHigh Authority Control lacLACLow Authority Control nassNASSNano Active Stabilization System asdASDAmplitude Spectral Density psdPSDPower Spectral Density cpsCPSCumulative Power Spectrum casCASCumulative Amplitude Spectrum frfFRFFrequency Response Function iffIFFIntegral Force Feedback rdcRDCRelative Damping Control drgaDRGADynamical Relative Gain Array hpfHPFhigh-pass filter lpfLPFlow-pass filter dofDoFdegrees-of-freedom psdxname=Φ_x,description=Power spectral density of signal x asdxname=Γ_x,description=Amplitude spectral density of signal x cpsxname=Φ_x,description=Cumulative Power Spectrum of signal x casxname=Γ_x,description=Cumulative Amplitude Spectrum of signal x

Test Bench - Amplified Piezoelectric Actuator

Dehaeze Thomas

October 29, 2024

Contents

In this chapter, the goal is to ensure that the received APA300ML (shown in Figure 1) are complying with the requirements and that the dynamical models of the actuator accurately represent its dynamics.

In section 1, the mechanical tolerances of the APA300ML interfaces are checked together with the electrical properties of the piezoelectric stacks and the achievable stroke. The flexible modes of the APA300ML, which were estimated using a finite element model, are compared with measurements.

Using a dedicated test bench, dynamical measurements are performed (Section 2). The dynamics from the generated DAC voltage (going through the voltage amplifier and then to two actuator stacks) to the induced axial displacement and to the measured voltage across the force sensor stack are estimated. Integral Force Feedback is experimentally applied, and the damped plants are estimated for several feedback gains.

Two different models of the APA300ML are presented. First, in Section 3, a two degrees-of-freedom model is presented, tuned, and compared with the measured dynamics. This model is proven to accurately represent the APA300ML's axial dynamics while having low complexity.

Then, in Section 4, a *super element* of the APA300ML is extracted using a finite element model and imported into Simscape. This more complex model also captures well capture the axial dynamics of the APA300ML.

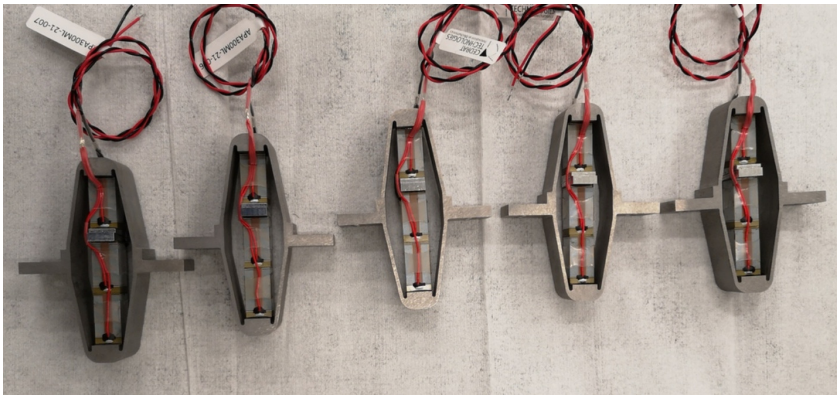

Figure 1: Picture of 5 out of the 7 received APA300ML

1 First Basic Measurements

Before measuring the dynamical characteristics of the APA300ML, simple measurements are performed. First, the tolerances (especially flatness) of the mechanical interfaces are checked in Section 1.1. Then, the capacitance of the piezoelectric stacks is measured in Section 1.2. The achievable stroke of the APA300ML is measured using a displacement probe in Section 1.3. Finally, in Section 1.4, the flexible modes of the APA are measured and compared with a finite element model.

1.1 Geometrical Measurements

To measure the flatness of the two mechanical interfaces of the APA300ML, a small measurement bench is installed on top of a metrology granite with excellent flatness. As shown in Figure 1.1, the APA is fixed to a clamp while a measuring probe[1] is used to measure the height of four points on each of the APA300ML interfaces. From the X-Y-Z coordinates of the measured eight points, the flatness is estimated by best fitting[2] a plane through all the points. The measured flatness values, summarized in Table 1.1, are within the specifications.

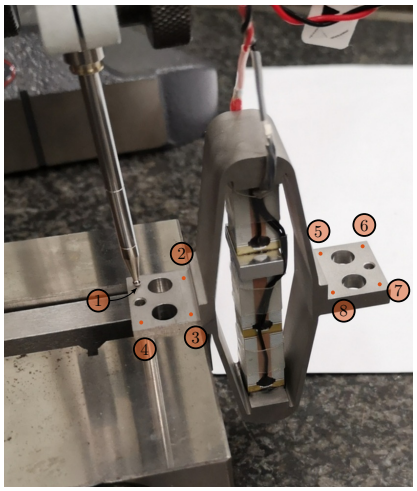

Figure 1.1: Measurement setup for flatness estimation

	Flatness $[\mu m]$
APA 1	8.9
APA 2	3.1
APA 3	9.1
APA 4	3.0
APA 5	1.9
APA 6	7.1
APA 7	18.7

Table 1.1: Estimated flatness of the APA300ML interfaces

[1] Heidenhain MT25, specified accuracy of $\pm 0.5\,\mu m$

[2] The Matlab `fminsearch` command is used to fit the plane

1.2 Electrical Measurements

From the documentation of the APA300ML, the total capacitance of the three stacks should be between $18\,\mu F$ and $26\,\mu F$ with a nominal capacitance of $20\,\mu F$.

The capacitance of the APA300ML piezoelectric stacks was measured with the LCR meter[3] shown in Figure 1.2. The two stacks used as the actuator and the stack used as the force sensor were measured separately. The measured capacitance values are summarized in Table 1.2 and the average capacitance of one stack is $\approx 5\mu F$. However, the measured capacitance of the stacks of "APA 3" is only half of the expected capacitance. This may indicate a manufacturing defect.

The measured capacitance is found to be lower than the specified value. This may be because the manufacturer measures the capacitance with large signals ($-20\,V$ to $150\,V$), whereas it was here measured with small signals [1].

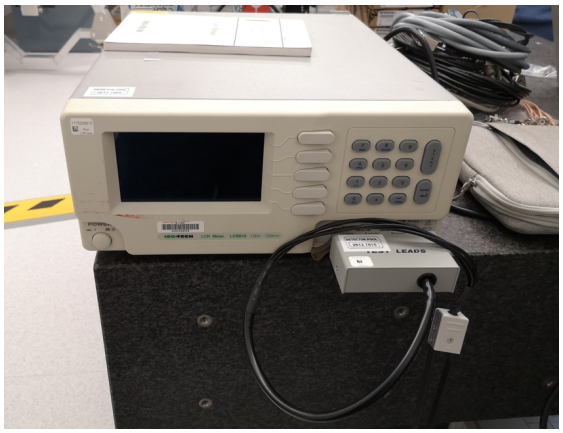

Figure 1.2: Used LCR meter

	Sensor Stack	Actuator Stacks
APA 1	5.10	10.03
APA 2	4.99	9.85
APA 3	1.72	5.18
APA 4	4.94	9.82
APA 5	4.90	9.66
APA 6	4.99	9.91
APA 7	4.85	9.85

Table 1.2: Measured capacitance in μF

1.3 Stroke and Hysteresis Measurement

To compare the stroke of the APA300ML with the datasheet specifications, one side of the APA is fixed to the granite, and a displacement probe[4] is located on the other side as shown in Figure 1.3.

The voltage across the two actuator stacks is varied from $-20\,V$ to $150\,V$ using a DAC[5] and a voltage amplifier[6]. Note that the voltage is slowly varied as the displacement probe has a very low measurement bandwidth (see Figure 1.4a).

The measured APA displacement is shown as a function of the applied voltage in Figure 1.4b. Typical hysteresis curves for piezoelectric stack actuators can be observed. The measured stroke is approximately $250\,\mu m$ when using only two of the three stacks. This is even above what is specified as the nominal stroke in the data-sheet ($304\,\mu m$, therefore $\approx 200\,\mu m$ if only two stacks are used). For the

[3] LCR-819 from Gwinstek, with a specified accuracy of 0.05%. The measured frequency is set at 1 kHz
[4] Millimar 1318 probe, specified linearity better than $1\,\mu m$
[5] The DAC used is the one included in the IO133 card sold by Speedgoat. It has an output range of $\pm 10\,V$ and 16-bits resolution
[6] PD200 from PiezoDrive. The gain is $20\,V/V$

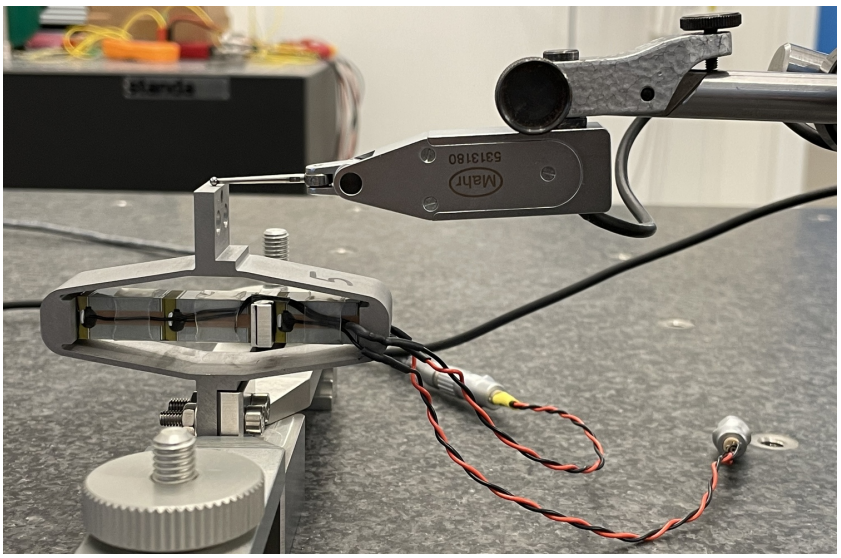

Figure 1.3: Bench to measure the APA stroke

NASS, this stroke is sufficient because the positioning errors to be corrected using the nano-hexapod are expected to be in the order of $10\,\mu m$.

It is clear from Figure 1.4b that "APA 3" has an issue compared with the other units. This confirms the abnormal electrical measurements made in Section 1.2. This unit was sent sent back to Cedrat, and a new one was shipped back. From now on, only the six remaining amplified piezoelectric actuators that behave as expected will be used.

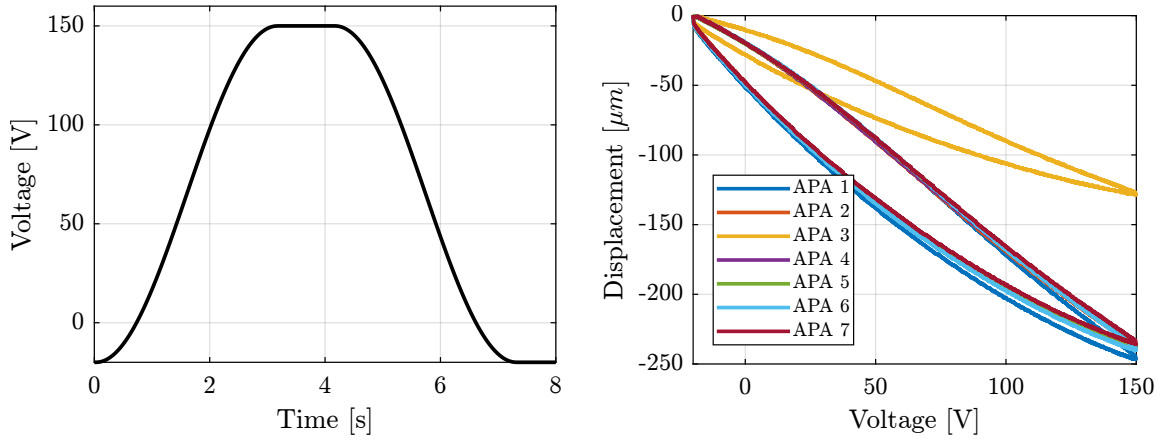

(a) Applied voltage for stroke estimation

(b) Hysteresis curves of the APA

Figure 1.4: Generated voltage across the two piezoelectric stack actuators to estimate the stroke of the APA300ML (a). Measured displacement as a function of applied voltage (b)

1.4 Flexible Mode Measurement

In this section, the flexible modes of the APA300ML are investigated both experimentally and using a Finite Element Model. To experimentally estimate these modes, the APA is fixed at one end (see Figure 1.6). A Laser Doppler Vibrometer[7] is used to measure the difference of motion between two "red" points and an instrumented hammer[8] is used to excite the flexible modes. Using this setup, the transfer function from the injected force to the measured rotation can be computed under different conditions, and the frequency and mode shapes of the flexible modes can be estimated.

The flexible modes for the same condition (i.e. one mechanical interface of the APA300ML fixed) are estimated using a finite element software, and the results are shown in Figure 1.5.

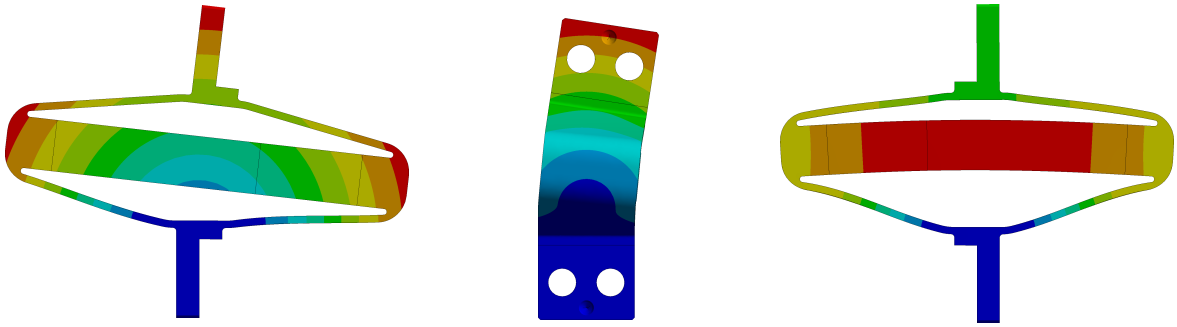

(a) Y-bending mode (268Hz) **(b)** X-bending mode (399Hz) **(c)** Z-axial mode (706Hz)

Figure 1.5: First three modes of the APA300ML in a fix-free condition estimated from a Finite Element Model

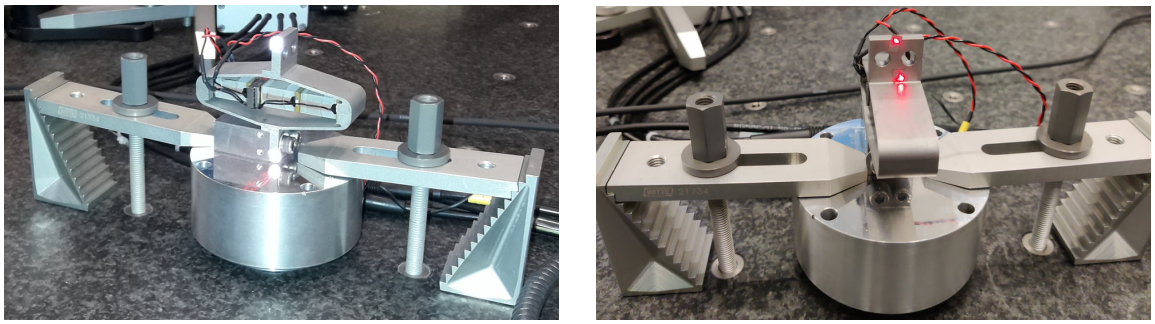

(a) X bending **(b)** Y Bending

Figure 1.6: Experimental setup to measure the flexible modes of the APA300ML. For the bending in the X direction (a), the impact point is at the back of the top measurement point. For the bending in the Y direction (b), the impact point is located on the back surface of the top interface (on the back of the 2 measurements points).

The measured frequency response functions computed from the experimental setups of figures 1.6a and 1.6b are shown in Figure 1.7. The y bending mode is observed at 280 Hz and the x bending mode is at 412 Hz. These modes are measured at higher frequencies than the frequencies estimated from the

[7] Polytec controller 3001 with sensor heads OFV512
[8] Kistler 9722A

Finite Element Model (see frequencies in Figure 1.5). This is the opposite of what is usually observed (i.e. having lower resonance frequencies in practice than the estimation from a finite element model). This could be explained by underestimation of the Young's modulus of the steel used for the shell (190 GPa was used for the model, but steel with Young's modulus of 210 GPa could have been used). Another explanation is the shape difference between the manufactured APA300ML and the 3D model, for instance thicker blades.

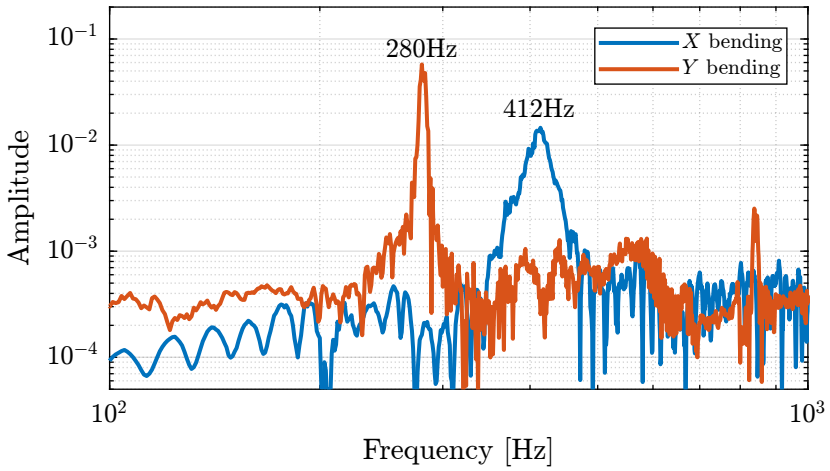

Figure 1.7: Frequency response functions for the two tests using the instrumented hammer and the laser vibrometer. The Y-bending mode is measured at 280 Hz and the X-bending mode at 412 Hz

2 Dynamical measurements

After the measurements on the APA were performed in Section 1, a new test bench was used to better characterize the dynamics of the APA300ML. This test bench, depicted in Figure 2.1, comprises the APA300ML fixed at one end to a stationary granite block and at the other end to a 5kg granite block that is vertically guided by an air bearing. Thus, there is no friction when actuating the APA300ML, and it will be easier to characterize its behavior independently of other factors. An encoder[1] is used to measure the relative movement between the two granite blocks, thereby measuring the axial displacement of the APA.

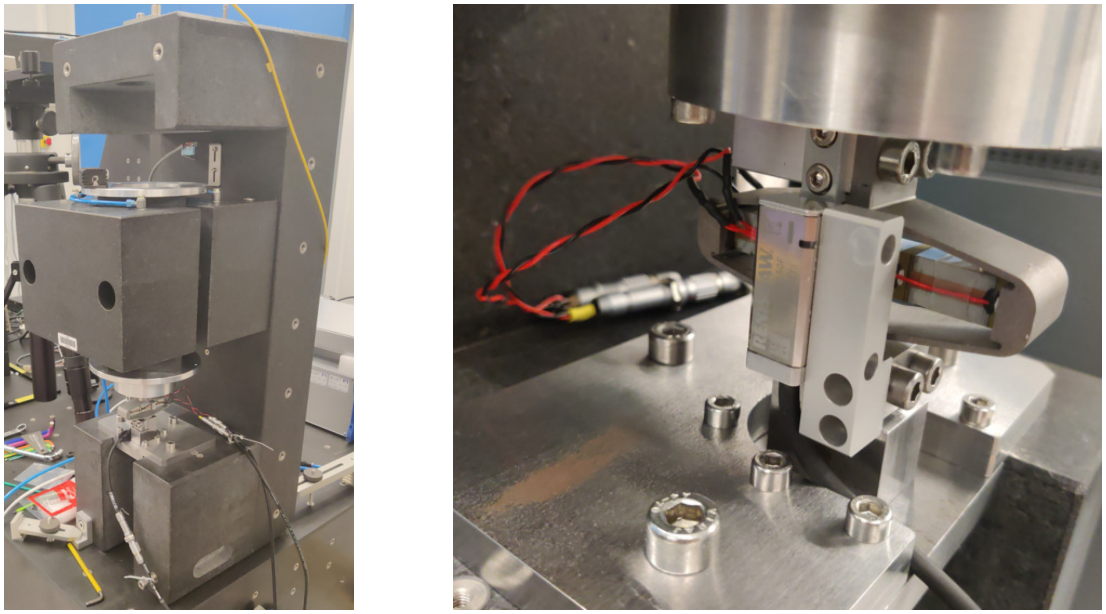

(a) Picture of the test bench **(b)** Zoom on the APA with the encoder

Figure 2.1: Schematic of the test bench used to estimate the dynamics of the APA300ML

The bench is schematically shown in Figure 2.2 with the associated signals. It will be first used to estimate the hysteresis from the piezoelectric stack (Section 2.1) as well as the axial stiffness of the APA300ML (Section 2.2). The frequency response functions from the DAC voltage u to the displacement d_e and to the voltage V_s are measured in Section 2.3. The presence of a non-minimum phase zero found on the transfer function from u to V_s is investigated in Section 2.4. To limit the low-frequency gain of the transfer function from u to V_s, a resistor is added across the force sensor stack (Section 2.5). Finally, the Integral Force Feedback is implemented, and the amount of damping added is experimentally estimated in Section 2.6.

[1] Renishaw Vionic, resolution of 2.5 nm

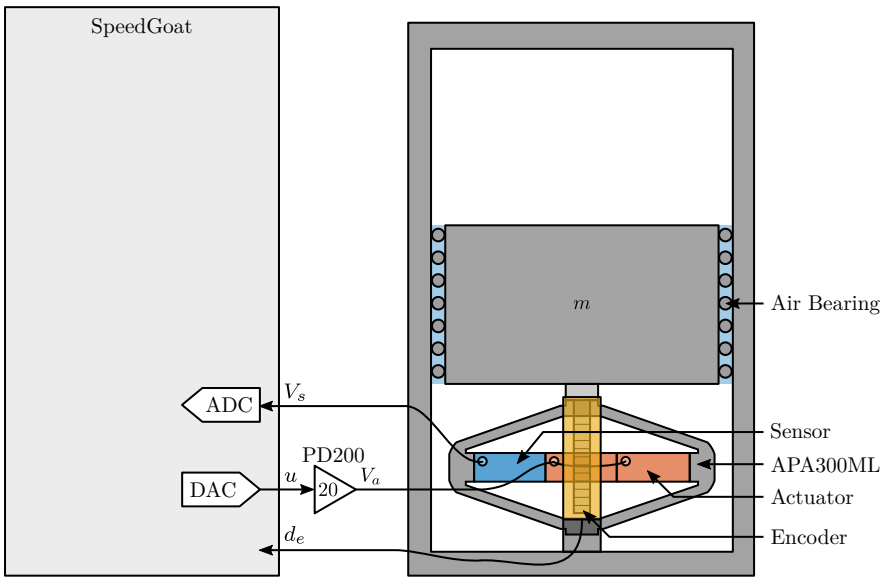

Figure 2.2: Schematic of the Test Bench used to measure the dynamics of the APA300ML. u is the output DAC voltage, V_a the output amplifier voltage (i.e. voltage applied across the actuator stacks), d_e the measured displacement by the encoder and V_s the measured voltage across the sensor stack.

2.1 Hysteresis

Because the payload is vertically guided without friction, the hysteresis of the APA can be estimated from the motion of the payload. A quasi static[2] sinusoidal excitation V_a with an offset of $65\,V$ (halfway between $-20\,V$ and $150\,V$) and with an amplitude varying from $4\,V$ up to $80\,V$ is generated using the DAC. For each excitation amplitude, the vertical displacement d_e of the mass is measured and displayed as a function of the applied voltage in Figure 2.3. This is the typical behavior expected from a PZT stack actuator, where the hysteresis increases as a function of the applied voltage amplitude [2, chap. 1.4].

2.2 Axial stiffness

To estimate the stiffness of the APA, a weight with known mass $m_a = 6.4\,\text{kg}$ is added on top of the suspended granite and the deflection Δd_e is measured using the encoder. The APA stiffness can then be estimated from equation (2.1), with $g \approx 9.8\,m/s^2$ the acceleration of gravity.

$$k_{\text{apa}} = \frac{m_a g}{\Delta d_e} \tag{2.1}$$

The measured displacement d_e as a function of time is shown in Figure 2.4. It can be seen that there are some drifts in the measured displacement (probably due to piezoelectric creep), and that the displacement does not return to the initial position after the mass is removed (probably due to piezoelectric hysteresis). These two effects induce some uncertainties in the measured stiffness.

[2] Frequency of the sinusoidal wave is 1 Hz

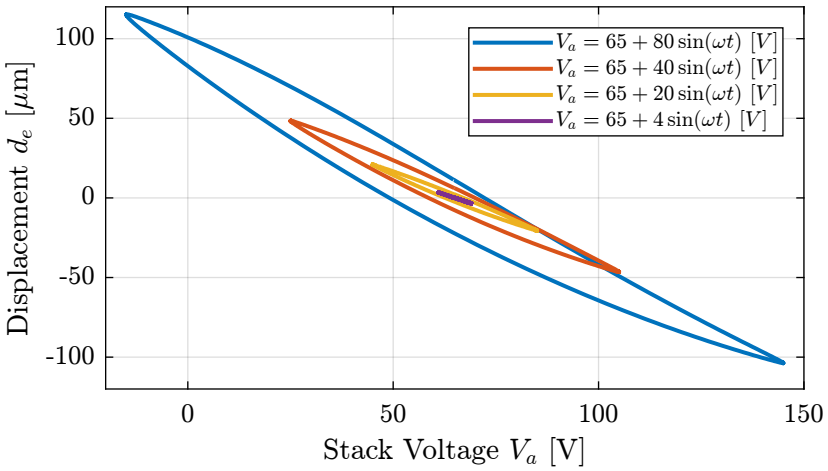

Figure 2.3: Displacement as a function of applied voltage for multiple excitation amplitudes

The stiffnesses are computed for all APAs from the two displacements d_1 and d_2 (see Figure 2.4) leading to two stiffness estimations k_1 and k_2. These estimated stiffnesses are summarized in Table 2.1 and are found to be close to the specified nominal stiffness of the APA300ML $k = 1.8\,N/\mu m$.

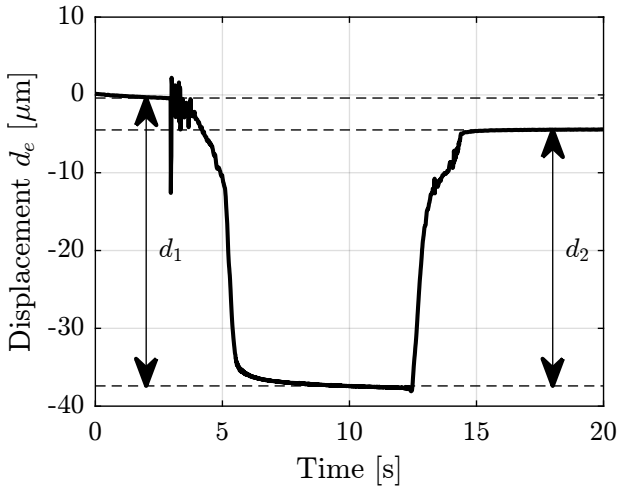

Figure 2.4: Measured displacement when adding (at $t \approx 3\,s$) and removing (at $t \approx 13\,s$) the mass

APA	k_1	k_2
1	1.68	1.9
2	1.69	1.9
4	1.7	1.91
5	1.7	1.93
6	1.7	1.92
8	1.73	1.98

Table 2.1: Measured axial stiffnesses (in $N/\mu m$)

The stiffness can also be computed using equation (2.2) by knowing the main vertical resonance frequency $\omega_z \approx 95\,\text{Hz}$ (estimated by the dynamical measurements shown in section 2.3) and the suspended mass $m_{\text{sus}} = 5.7\,\text{kg}$.

$$\omega_z = \sqrt{\frac{k}{m_{\text{sus}}}} \tag{2.2}$$

The obtained stiffness is $k \approx 2\,N/\mu m$ which is close to the values found in the documentation and using the "static deflection" method.

It is important to note that changes to the electrical impedance connected to the piezoelectric stacks affect the mechanical compliance (or stiffness) of the piezoelectric stack [3, chap. 2].

To estimate this effect for the APA300ML, its stiffness is estimated using the "static deflection" method in two cases:

- k_{os}: piezoelectric stacks left unconnected (or connect to the high impedance ADC)
- k_{sc}: piezoelectric stacks short-circuited (or connected to the voltage amplifier with small output impedance)

The open-circuit stiffness is estimated at $k_{\text{oc}} \approx 2.3\,N/\mu m$ while the closed-circuit stiffness $k_{\text{sc}} \approx 1.7\,N/\mu m$.

2.3 Dynamics

In this section, the dynamics from the excitation voltage u to the encoder measured displacement d_e and to the force sensor voltage V_s is identified.

First, the dynamics from u to d_e for the six APA300ML are compared in Figure 2.5a. The obtained frequency response functions are similar to those of a (second order) mass-spring-damper system with:

- A "stiffness line" indicating a static gain equal to $\approx -17\,\mu m/V$. The negative sign comes from the fact that an increase in voltage stretches the piezoelectric stack which reduces the height of the APA
- A lightly damped resonance at 95 Hz
- A "mass line" up to ≈ 800 Hz, above which additional resonances appear. These additional resonances might be due to the limited stiffness of the encoder support or from the limited compliance of the APA support. The flexible modes studied in section 1.4 seem not to impact the measured axial motion of the actuator.

The dynamics from u to the measured voltage across the sensor stack V_s for the six APA300ML are compared in Figure 2.5b.

A lightly damped resonance (pole) is observed at 95 Hz and a lightly damped anti-resonance (zero) at 41 Hz. No additional resonances are present up to at least 2 kHz indicating that Integral Force Feedback can be applied without stability issues from high-frequency flexible modes. The zero at 41 Hz seems to be non-minimum phase (the phase *decreases* by 180 degrees whereas it should have *increased* by 180 degrees for a minimum phase zero). This is investigated in Section 2.4.

As illustrated by the Root Locus plot, the poles of the *closed-loop* system converges to the zeros of the *open-loop* plant as the feedback gain increases. The significance of this behavior varies with the type of sensor used, as explained in [4, chap. 7.6]. Considering the transfer function from u to V_s, if a controller with a very high gain is applied such that the sensor stack voltage V_s is kept at zero, the sensor (and by extension, the actuator stacks since they are in series) experiences negligible stress and strain. Consequently, the closed-loop system virtually corresponds to one in which the piezoelectric stacks are absent, leaving only the mechanical shell. From this analysis, it can be inferred that the axial

stiffness of the shell is $k_{\text{shell}} = m\omega_0^2 = 5.7 \cdot (2\pi \cdot 41)^2 = 0.38\, N/\mu m$ (which is close to what is found using a finite element model).

All the identified dynamics of the six APA300ML (both when looking at the encoder in Figure 2.5a and at the force sensor in Figure 2.5b) are almost identical, indicating good manufacturing repeatability for the piezoelectric stacks and the mechanical shell.

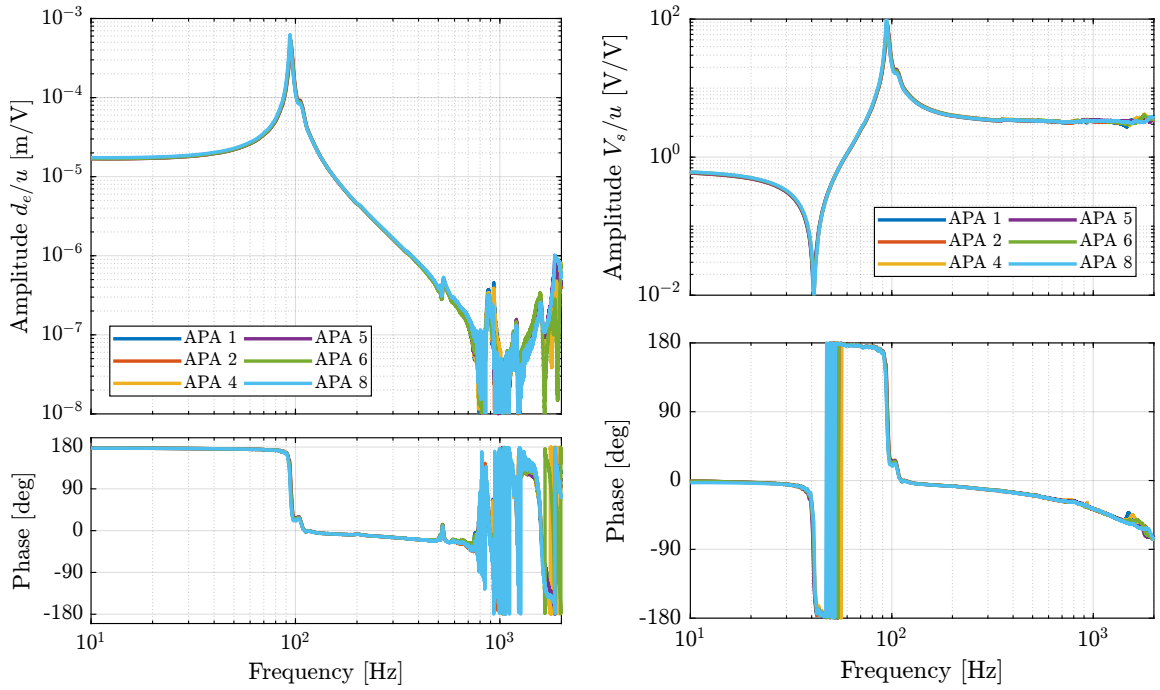

(a) FRF from u to d_e

(b) FRF from u to V_s

Figure 2.5: Measured frequency response function from generated voltage u to the encoder displacement d_e (a) and to the force sensor voltage V_s (b) for the six APA300ML

2.4 Non Minimum Phase Zero?

It was surprising to observe a non-minimum phase zero on the transfer function from u to V_s (Figure 2.5b). It was initially thought that this non-minimum phase behavior was an artifact arising from the measurement. A longer measurement was performed using different excitation signals (noise, slow sine sweep, etc.) to determine if the phase behavior of the zero changes (Figure 2.6). The coherence (Figure 2.6a) is good even in the vicinity of the lightly damped zero, and the phase (Figure 2.6b) clearly indicates non-minimum phase behavior.

Such non-minimum phase zero when using load cells has also been observed on other mechanical systems [5–7]. It could be induced to small non-linearity in the system, but the reason for this non-minimum phase for the APA300ML is not yet clear.

However, this is not so important here because the zero is lightly damped (i.e. very close to the imaginary axis), and the closed loop poles (see the Root Locus plot in Figure 2.10b) should not be unstable, except for very large controller gains that will never be applied in practice.

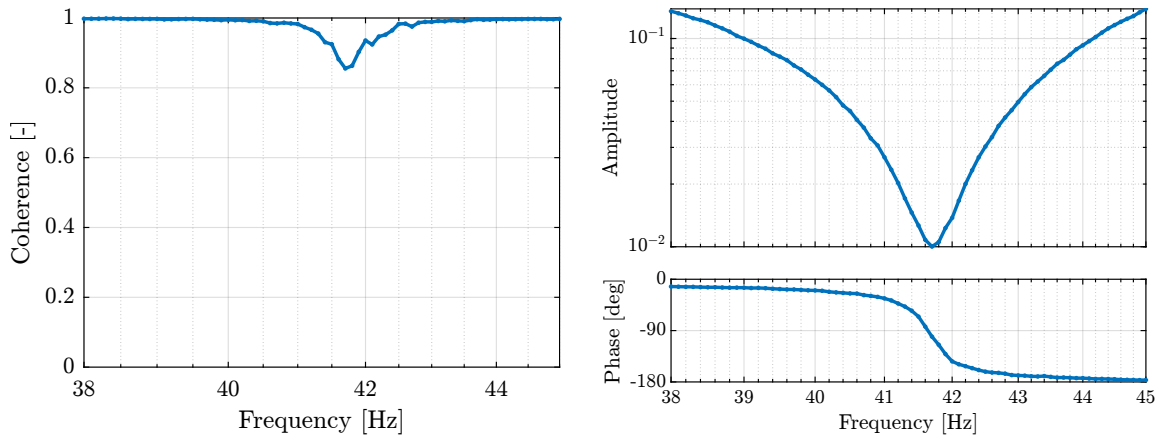

(a) Coherence

(b) Zoom on the non-minimum phase zero

Figure 2.6: Measurement of the anti-resonance found in the transfer function from u to V_s. The coherence (a) is quite good around the anti-resonance frequency. The phase (b) shoes a non-minimum phase behavior.

2.5 Effect of the resistor on the IFF Plant

A resistor $R \approx 80.6\,k\Omega$ is added in parallel with the sensor stack, which forms a high-pass filter with the capacitance of the piezoelectric stack (capacitance estimated at $\approx 5\,\mu F$).

As explained before, this is done to limit the voltage offset due to the input bias current of the ADC as well as to limit the low frequency gain.

The (low frequency) transfer function from u to V_s with and without this resistor were measured and compared in Figure 2.7. It is confirmed that the added resistor has the effect of adding a high-pass filter with a cut-off frequency of $\approx 0.39\,\text{Hz}$.

2.6 Integral Force Feedback

To implement the Integral Force Feedback strategy, the measured frequency response function from u to V_s (Figure 2.5b) is fitted using the transfer function shown in equation (2.3). The parameters were manually tuned, and the obtained values are $\omega_{\text{HPF}} = 0.4\,\text{Hz}$, $\omega_z = 42.7\,\text{Hz}$, $\xi_z = 0.4\,\%$, $\omega_p = 95.2\,\text{Hz}$, $\xi_p = 2\,\%$ and $g_0 = 0.64$.

$$G_{\text{IFF},m}(s) = g_0 \cdot \frac{1 + 2\xi_z \frac{s}{\omega_z} + \frac{s^2}{\omega_z^2}}{1 + 2\xi_p \frac{s}{\omega_p} + \frac{s^2}{\omega_p^2}} \cdot \frac{s}{\omega_{\text{HPF}} + s} \tag{2.3}$$

A comparison between the identified plant and the manually tuned transfer function is shown in Figure 2.8.

The implemented Integral Force Feedback Controller transfer function is shown in equation (2.4). It

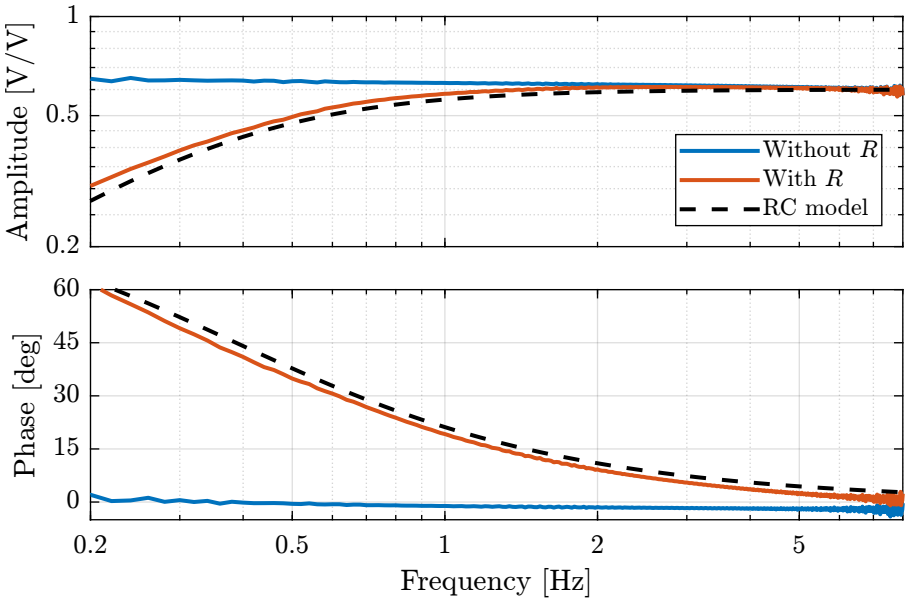

Figure 2.7: Transfer function from u to V_s with and without the resistor R in parallel with the piezoelectric stack used as the force sensor

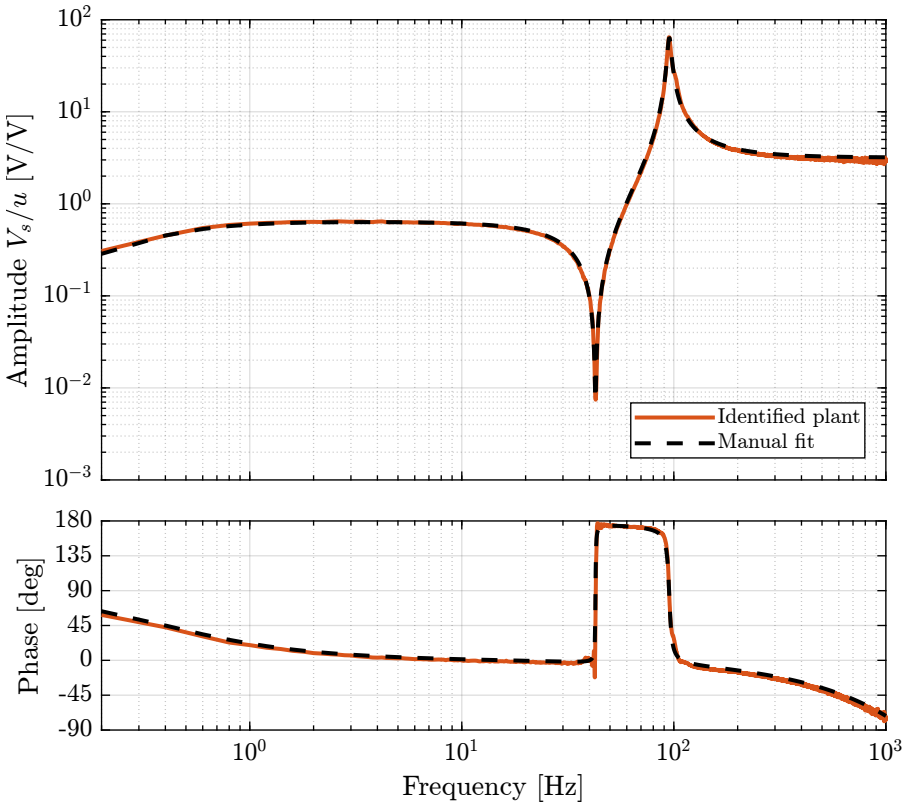

Figure 2.8: Identified IFF plant and manually tuned model of the plant (a time delay of 200 μs is added to the model of the plant to better match the identified phase). Note that a minimum-phase zero is identified here even though the coherence is not good around the frequency of the zero.

contains a high-pass filter (cut-off frequency of 2 Hz) to limit the low-frequency gain, a low-pass filter to add integral action above 20 Hz, a second low-pass filter to add robustness to high-frequency resonances, and a tunable gain g.

$$K_{\text{IFF}}(s) = -10 \cdot g \cdot \frac{s}{s + 2\pi \cdot 2} \cdot \frac{1}{s + 2\pi \cdot 20} \cdot \frac{1}{s + 2\pi \cdot 2000} \tag{2.4}$$

To estimate how the dynamics of the APA changes when the Integral Force Feedback controller is implemented, the test bench shown in Figure 2.9 is used. The transfer function from the "damped" plant input $u\prime$ to the encoder displacement d_e is identified for several IFF controller gains g.

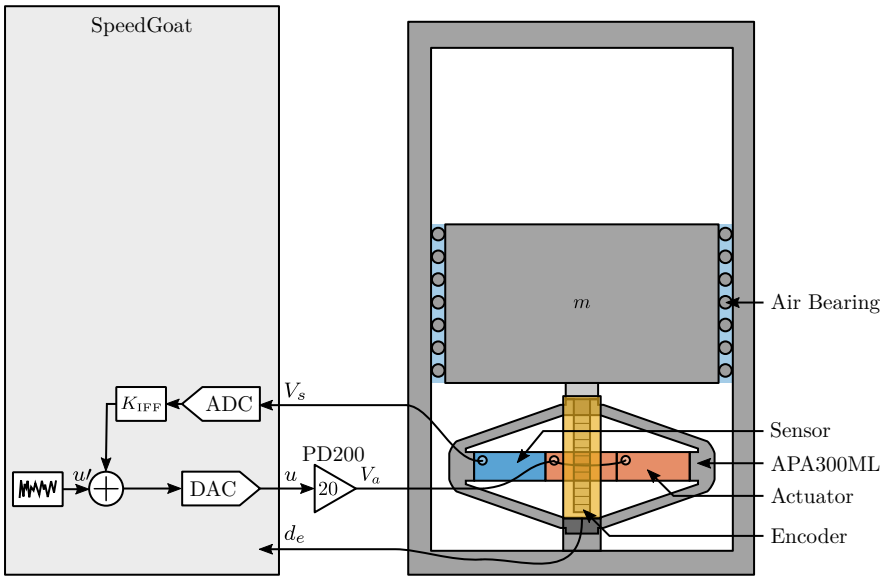

Figure 2.9: Implementation of Integral Force Feedback in the Speedgoat. The damped plant has a new input $u\prime$

The identified dynamics were then fitted by second order transfer functions[3]. A comparison between the identified damped dynamics and the fitted second-order transfer functions is shown in Figure 2.10a for different gains g. It is clear that a large amount of damping is added when the gain is increased and that the frequency of the pole is shifted to lower frequencies.

The evolution of the pole in the complex plane as a function of the controller gain g (i.e. the "root locus") is computed in two cases. First using the IFF plant model (2.3) and the implemented controller (2.4). Second using the fitted transfer functions of the damped plants experimentally identified for several controller gains. The two obtained root loci are compared in Figure 2.10b and are in good agreement considering that the damped plants were fitted using only a second-order transfer function.

[3]The transfer function fitting was computed using the `vectfit3` routine, see [8]

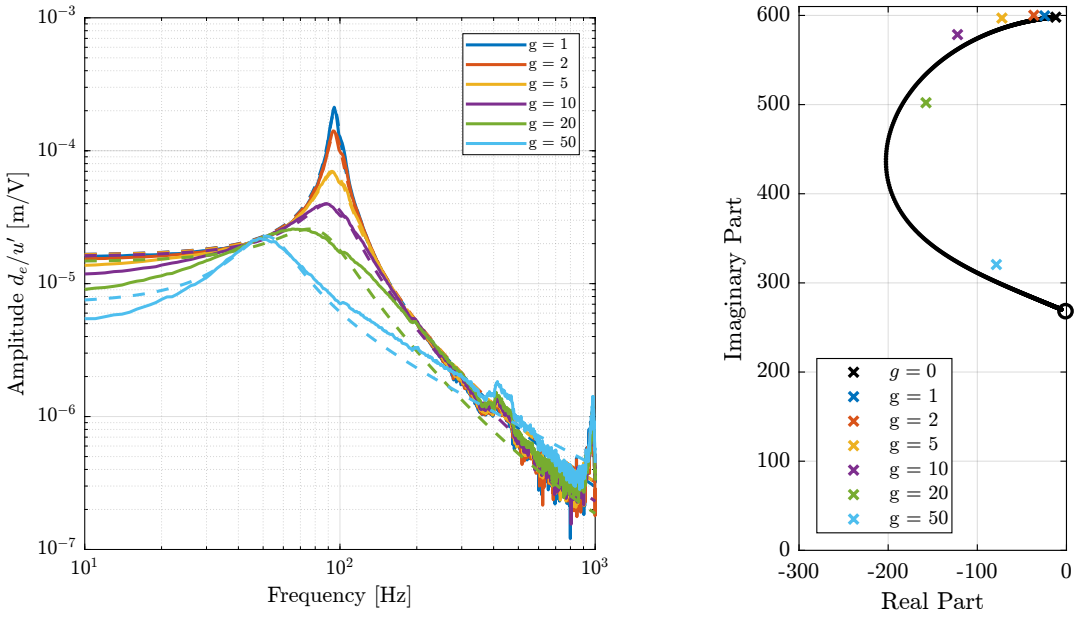

(a) Measured frequency response functions of damped plants for several IFF gains (solid lines). Identified 2nd order plants that match the experimental data (dashed lines)

(b) Root Locus plot using the plant model (black) and poles of the identified damped plants (color crosses)

Figure 2.10: Experimental results of applying Integral Force Feedback to the APA300ML. Obtained damped plant (a) and Root Locus (b) corresponding to the implemented IFF controller (2.4)

3 APA300ML - 2 degrees-of-freedom Model

In this section, a Simscape model (Figure 3.1) of the measurement bench is used to tune the two degrees-of-freedom model of the APA using the measured frequency response functions.

This two degrees-of-freedom model is developed to accurately represent the APA300ML dynamics while having low complexity and a low number of associated states. After the model is presented, the procedure for tuning the model is described, and the obtained model dynamics is compared with the measurements.

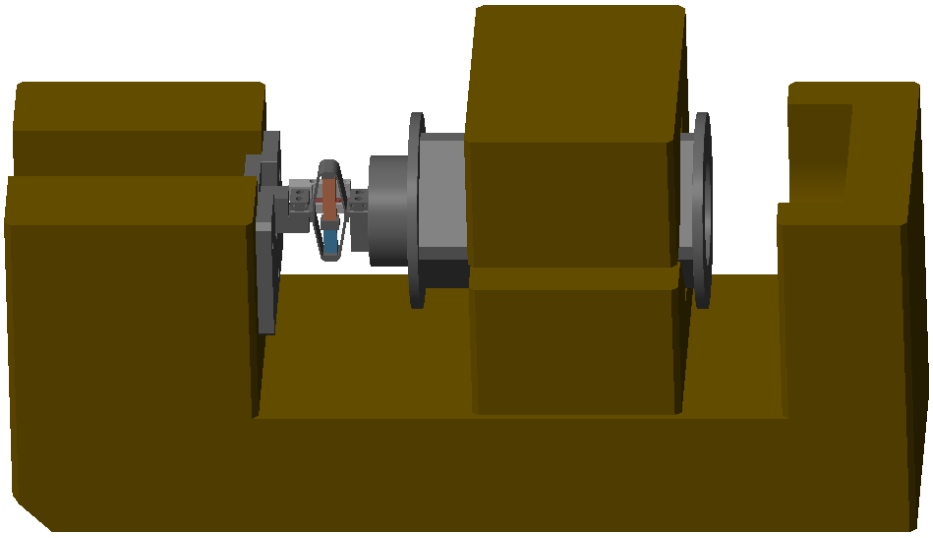

Figure 3.1: Screenshot of the Simscape model

Two degrees-of-freedom APA Model The model of the amplified piezoelectric actuator is shown in Figure 3.2. It can be decomposed into three components:

- the shell whose axial properties are represented by k_1 and c_1
- the actuator stacks whose contribution to the axial stiffness is represented by k_a and c_a. The force source τ represents the axial force induced by the force sensor stacks. The sensitivity g_a (in N/m) is used to convert the applied voltage V_a to the axial force τ
- the sensor stack whose contribution to the axial stiffness is represented by k_e and c_e. A sensor measures the stack strain d_e which is then converted to a voltage V_s using a sensitivity g_s (in V/m)

Such a simple model has some limitations:

- it only represents the axial characteristics of the APA as it is modeled as infinitely rigid in the other directions
- some physical insights are lost, such as the amplification factor and the real stress and strain in the piezoelectric stacks
- the creep and hysteresis of the piezoelectric stacks are not modeled as the model is linear

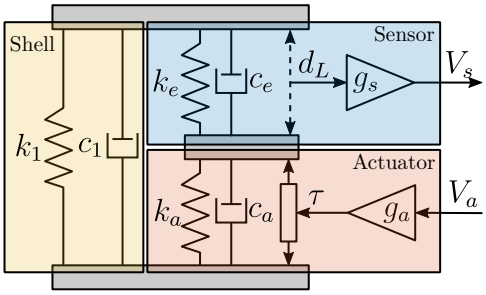

Figure 3.2: Schematic of the two degrees-of-freedom model of the APA300ML, adapted from [9]

9 parameters (m, k_1, c_1, k_e, c_e, k_a, c_a, g_s and g_a) have to be tuned such that the dynamics of the model (Figure 3.3) well represents the identified dynamics in Section 2.

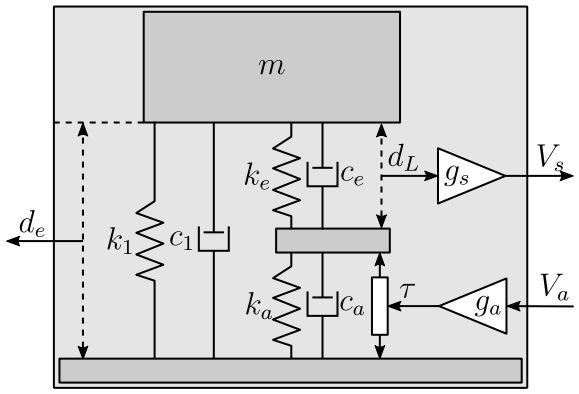

Figure 3.3: Schematic of the two degrees-of-freedom model of the APA300ML with input V_a and outputs d_e and V_s

First, the mass m supported by the APA300ML can be estimated from the geometry and density of the different parts or by directly measuring it using a precise weighing scale. Both methods lead to an estimated mass of $m = 5.7\,\text{kg}$.

Then, the axial stiffness of the shell was estimated at $k_1 = 0.38\,N/\mu m$ in Section 2.3 from the frequency of the anti-resonance seen on Figure 2.5b. Similarly, c_1 can be estimated from the damping ratio of the same anti-resonance and is found to be close to $5\,Ns/m$.

Then, it is reasonable to assume that the sensor stacks and the two actuator stacks have identical mechanical characteristics[1]. Therefore, we have $k_e = 2k_a$ and $c_e = 2c_a$ as the actuator stack is composed

[1]Note that this is not completely correct as it was shown in Section 2.2 that the electrical boundaries of the piezoelectric stack impacts its stiffness and that the sensor stack is almost open-circuited while the actuator stacks are almost

of two stacks in series. In this case, the total stiffness of the APA model is described by (3.1).

$$k_{\text{tot}} = k_1 + \frac{k_e k_a}{k_e + k_a} = k_1 + \frac{2}{3} k_a \tag{3.1}$$

Knowing from (3.2) that the total stiffness is $k_{\text{tot}} = 2\,N/\mu m$, we get from (3.1) that $k_a = 2.5\,N/\mu m$ and $k_e = 5\,N/\mu m$.

$$\omega_0 = \frac{k_{\text{tot}}}{m} \Longrightarrow k_{\text{tot}} = m\omega_0^2 = 2\,N/\mu m \quad \text{with } m = 5.7\,\text{kg and } \omega_0 = 2\pi \cdot 95\,\text{rad}/s \tag{3.2}$$

Then, c_a (and therefore $c_e = 2c_a$) can be tuned to match the damping ratio of the identified resonance. $c_a = 50\,Ns/m$ and $c_e = 100\,Ns/m$ are obtained.

In the last step, g_s and g_a can be tuned to match the gain of the identified transfer functions.

The obtained parameters of the model shown in Figure 3.3 are summarized in Table 3.1.

Parameter	**Value**
m	$5.7\,\text{kg}$
k_1	$0.38\,N/\mu m$
k_e	$5.0\,N/\mu m$
k_a	$2.5\,N/\mu m$
c_1	$5\,Ns/m$
c_e	$100\,Ns/m$
c_a	$50\,Ns/m$
g_a	$-2.58\,N/V$
g_s	$0.46\,V/\mu m$

Table 3.1: Summary of the obtained parameters for the 2 DoF APA300ML model

The dynamics of the two degrees-of-freedom model of the APA300ML are extracted using optimized parameters (listed in Table 3.1) from the Simscape model. This is compared with the experimental data in Figure 3.4. A good match can be observed between the model and the experimental data, both for the encoder (Figure 3.4a) and for the force sensor (Figure 3.4b). This indicates that this model represents well the axial dynamics of the APA300ML.

short-circuited.

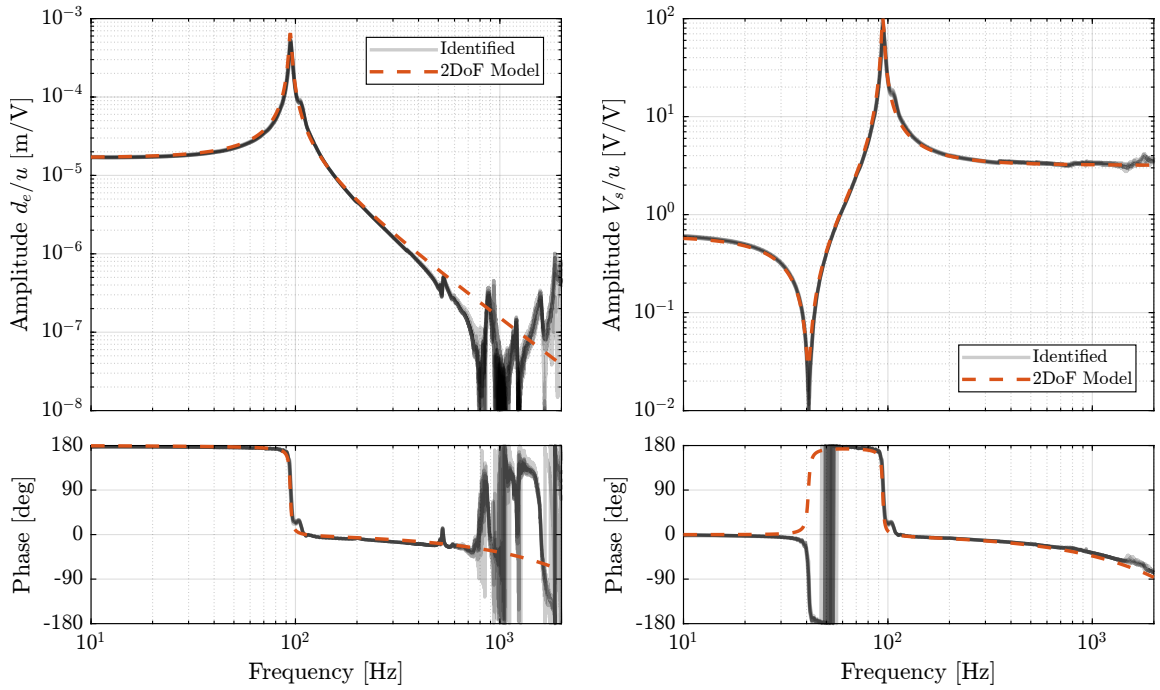

(a) from u to d_e **(b)** from u to V_s

Figure 3.4: Comparison of the measured frequency response functions and the identified dynamics from the 2DoF model of the APA300ML. Both for the dynamics from u to d_e (a) (b) and from u to V_s (b)

4 APA300ML - Super Element

In this section, a *super element* of the APA300ML is computed using a finite element software[1]. It is then imported into Simscape (in the form of a stiffness matrix and a mass matrix) and included in the same model that was used in 3. This procedure is illustrated in Figure 4.1. Several *remote points* are defined in the finite element model (here illustrated by colorful planes and numbers from 1 to 5) and are then made accessible in the Simscape model as shown at the right by the "frames" F1 to F5.

For the APA300ML *super element*, 5 *remote points* are defined. Two *remote points* (1 and 2) are fixed to the top and bottom mechanical interfaces of the APA300ML and will be used to connect the APA300ML with other mechanical elements. Two *remote points* (3 and 4) are located across two piezoelectric stacks and are used to apply internal forces representing the actuator stacks. Finally, two *remote points* (4 and 4) are located across the third piezoelectric stack, and will be used to measured the strain of the sensor stack.

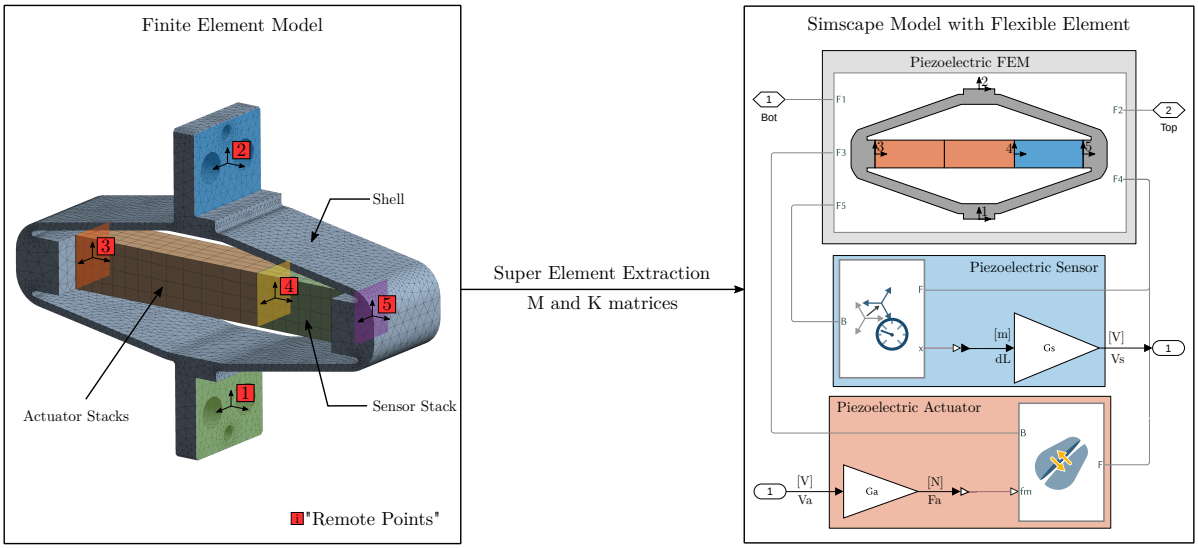

Figure 4.1: Finite Element Model of the APA300ML with "remotes points" on the left. Simscape model with included "Reduced Order Flexible Solid" on the right.

Identification of the Actuator and Sensor constants Once the APA300ML *super element* is included in the Simscape model, the transfer function from F_a to d_L and d_e can be extracted. The gains g_a and g_s are then tuned such that the gains of the transfer functions match the identified ones. By doing so, $g_s = 4.9\,V/\mu m$ and $g_a = 23.2\,N/V$ are obtained.

To ensure that the sensitivities g_a and g_s are physically valid, it is possible to estimate them from the physical properties of the piezoelectric stack material.

[1] Ansys® was used

From [2, p. 123], the relation between relative displacement d_L of the sensor stack and generated voltage V_s is given by (4.1a) and from [10] the relation between the force F_a and the applied voltage V_a is given by (4.1b).

$$V_s = \underbrace{\frac{d_{33}}{\epsilon^T s^D n}}_{g_s} d_L \tag{4.1a}$$

$$F_a = \underbrace{d_{33} n k_a}_{g_a} \cdot V_a, \quad k_a = \frac{c^E A}{L} \tag{4.1b}$$

Unfortunately, the manufacturer of the stack was not willing to share the piezoelectric material properties of the stack used in the APA300ML. However, based on the available properties of the APA300ML stacks in the data-sheet, the soft Lead Zirconate Titanate "THP5H" from Thorlabs seemed to match quite well the observed properties. The properties of this "THP5H" material used to compute g_a and g_s are listed in Table 4.1.

From these parameters, $g_s = 5.1\,V/\mu m$ and $g_a = 26\,N/V$ were obtained, which are close to the constants identified using the experimentally identified transfer functions.

Parameter	Value	Description
d_{33}	$680 \cdot 10^{-12}\,m/V$	Piezoelectric constant
ϵ^T	$4.0 \cdot 10^{-8}\,F/m$	Permittivity under constant stress
s^D	$21 \cdot 10^{-12}\,m^2/N$	Elastic compliance understand constant electric displacement
c^E	$48 \cdot 10^9\,N/m^2$	Young's modulus of elasticity
L	$20\,mm$ per stack	Length of the stack
A	$10^{-4}\,m^2$	Area of the piezoelectric stack
n	160 per stack	Number of layers in the piezoelectric stack

Table 4.1: Piezoelectric properties used for the estimation of the sensor and actuators sensitivities

Comparison of the obtained dynamics The obtained dynamics using the *super element* with the tuned "sensor sensitivity" and "actuator sensitivity" are compared with the experimentally identified frequency response functions in Figure 4.2. A good match between the model and the experimental results was observed. It is however surprising that the model is "softer" than the measured system, as finite element models usually overestimate the stiffness (see Section 1.4 for possible explanations).

Using this simple test bench, it can be concluded that the *super element* model of the APA300ML captures the axial dynamics of the actuator (the actuator stacks, the force sensor stack as well as the shell used as a mechanical lever).

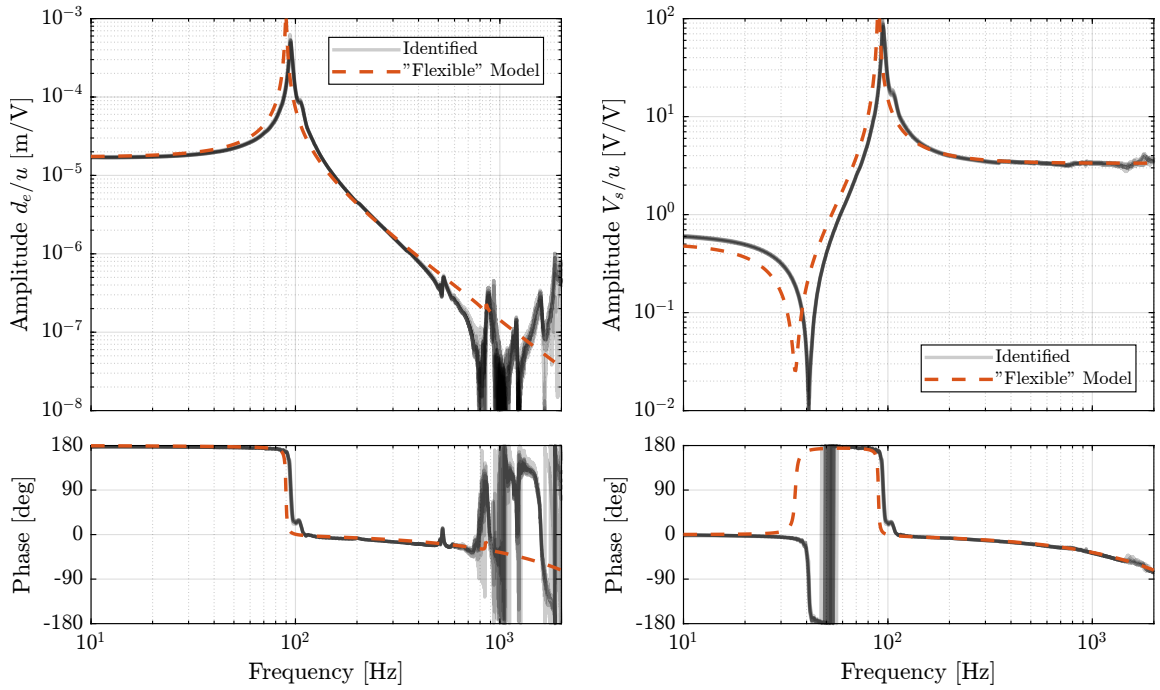

(a) from u to d_e

(b) from u to V_s

Figure 4.2: Comparison of the measured frequency response functions and the identified dynamics from the finite element model of the APA300ML. Both for the dynamics from u to d_e (a) and from u to V_s (b)

5 Conclusion

In this study, the amplified piezoelectric actuators "APA300ML" have been characterized to ensure that they fulfill all the requirements determined during the detailed design phase.

Geometrical features such as the flatness of its interfaces, electrical capacitance, and achievable strokes were measured in Section 1. These simple measurements allowed for the early detection of a manufacturing defect in one of the APA300ML.

Then in Section 2, using a dedicated test bench, the dynamics of all the APA300ML were measured and were found to all match very well (Figure 2.5). This consistency indicates good manufacturing tolerances, facilitating the modeling and control of the nano-hexapod. Although a non-minimum zero was identified in the transfer function from u to V_s (Figure 2.6), it was found not to be problematic because a large amount of damping could be added using the integral force feedback strategy (Figure 2.10).

Then, two different models were used to represent the APA300ML dynamics. In Section 3, a simple two degrees-of-freedom mass-spring-damper model was presented and tuned based on the measured dynamics. After following a tuning procedure, the model dynamics was shown to match very well with the experiment. However, this model only represents the axial dynamics of the actuators, assuming infinite stiffness in other directions.

In Section 4, a *super element* extracted from a finite element model was used to model the APA300ML. Here, the *super element* represents the dynamics of the APA300ML in all directions. However, only the axial dynamics could be compared with the experimental results, yielding a good match. The benefit of employing this model over the two degrees-of-freedom model is not immediately apparent due to its increased complexity and the larger number of model states involved. Nonetheless, the *super element* model's value will become clear in subsequent sections, when its capacity to accurately model the APA300ML's flexibility across various directions will be important.

Bibliography

[1] E. Wehrsdorfer, G. Borchhardt, W. Karthe, and G. Helke, "Large signal measurements on piezoelectric stacks," *Ferroelectrics*, vol. 174, no. 1, pp. 259–275, 1995 (cit. on p. 5).

[2] A. J. Fleming and K. K. Leang, *Design, Modeling and Control of Nanopositioning Systems* (Advances in Industrial Control). Springer International Publishing, 2014 (cit. on pp. 10, 23).

[3] M. Reza and F. Andrew, *Piezoelectric Transducers for Vibration Control and Damping*. London: Springer, 2006 (cit. on p. 12).

[4] A. Preumont, *Vibration Control of Active Structures - Fourth Edition* (Solid Mechanics and Its Applications). Springer International Publishing, 2018 (cit. on p. 12).

[5] J. Spanos, Z. Rahman, and G. Blackwood, "A soft 6-axis active vibration isolator," in *Proceedings of 1995 American Control Conference - ACC'95*, 1995 (cit. on p. 13).

[6] D. Thayer, M. Campbell, J. Vagners, and A. von Flotow, "Six-axis vibration isolation system using soft actuators and multiple sensors," *Journal of Spacecraft and Rockets*, vol. 39, no. 2, pp. 206–212, 2002 (cit. on p. 13).

[7] G. Hauge and M. Campbell, "Sensors and control of a space-based six-axis vibration isolation system," *Journal of Sound and Vibration*, vol. 269, no. 3-5, pp. 913–931, 2004 (cit. on p. 13).

[8] A. Gustavsen B.; Semlyen, "Rational approximation of frequency domain responses by vector fitting," *IEEE Transactions on Power Delivery*, vol. 14, 3 Jul. 1999 (cit. on p. 16).

[9] A. Souleille, T. Lampert, V. Lafarga, *et al.*, "A concept of active mount for space applications," *CEAS Space Journal*, vol. 10, no. 2, pp. 157–165, 2018 (cit. on p. 19).

[10] A. J. Fleming and K. K. Leang, "Integrated strain and force feedback for high-performance control of piezoelectric actuators," *Sensors and Actuators A: Physical*, vol. 161, no. 1-2, pp. 256–265, 2010 (cit. on p. 23).